Article

Not peer-reviewed version

Cryoelectrospun Elastin-Alginate Scaffolds Support In Vitro 3D Epithelial-Stromal Cocultures for Salivary Tissue Engineering

Pujhitha Ramesh *, James Castracane, Melinda Larsen, Deirdre A. Nelson, Susan T. Sharfstein, Yubing Xie *

Posted Date: 6 November 2025

doi: 10.20944/preprints202511.0438.v1

Keywords: cryoelectrospinning; alginate; elastin; extracellular matrix; 3D porous scaffold; 3D coculture; epithelial-stromal coculture; salivary gland tissue engineering

 doi:10.20944/preprints202511.0438.v1

Article

Cryoelectrospun Elastin-Alginate Scaffolds Support In Vitro 3D Epithelial-Stromal Cocultures for Salivary Tissue Engineering

Pujhitha Ramesh [1,*], James Castracane [1], Melinda Larsen [2,3], Deirdre A Nelson [2,3], Susan Sharfstein [1,3] and Yubing Xie [2,*]

[1] Department of Nanoscale Science and Engineering, College of Nanotechnology, Science, and Engineering, University at Albany, State University of New York (SUNY), Albany, New York 12203, USA
[2] Department of Biological Sciences, State University of New York, University at Albany, SUNY, Albany, New York 12222, USA
[3] The RNA Institute, State University of New York, University at Albany, SUNY, Albany, New York 12222, USA
* Correspondence: PR, pramesh@albany.edu; YX, yxie@albany.edu

Abstract

Bioengineered functional salivary tissues can advance regenerative therapies, preclinical drug testing, and fundamental understanding of salivary gland dysfunction. Current salivary tissue models are typically Matrigel-based, hydrogel-based or scaffold-free organoid systems, with limited physiological relevance or mimicry of cell-cell and cell-extracellular matrix (ECM) interactions. We previously developed elastin-alginate cryoelectrospun scaffolds (CES) that resemble the topography and viscoelastic properties of healthy salivary ECM, and validated their potential for stromal cell culture, delivery, and *in vitro* fibrosis modeling. Here, we evaluated the utility of CES to support 3D cocultures of salivary gland epithelial and mesenchymal cells *in vitro*. We compared CES with honeycomb-like topography (CES-H) to densely packed electrospun nanofibers (NF) and CES with fibrous topography (CES-F) for their ability to support SIMS epithelial cell attachment, morphology, 3D clustering, phenotype and organization into distinct clusters when cocultured with stromal cells. Both CES-F and CES-H supported epithelial cell attachment and clustering; in particular, CES-H most effectively supported the self-organization of epithelial and stromal cells into distinct 3D clusters resembling the structure of native salivary tissue. Stromal cells were essential for maintaining the phenotype of epithelial cells cultured on CES-H, laying the foundation for development of *in vitro* tissue models.

Keywords: cryoelectrospinning; alginate; elastin; extracellular matrix; 3D porous scaffold; 3D coculture; epithelial-stromal coculture; salivary gland tissue engineering

1. Introduction

The salivary gland is essential for oral and digestive health but can be impacted by pathologies, leading to salivary gland hypofunction, hyperfunction, and cancer [1]. Current treatment options for salivary gland dysfunction are largely palliative [2] and offer minimal relief, highlighting the need for curative therapies based on a comprehensive understanding of the fundamental mechanisms governing disease pathology.

Animal models, Matrigel™ or other hydrogel-based *in vitro* cell culture systems, and organoids are currently employed to study both salivary gland development and disease mechanisms [3–23]. While mouse models are often employed to study disease pathways and test therapeutic candidates, they are expensive, time-consuming, and poorly reflect human physiology, resulting in high failure rates of therapeutic candidates in clinical trials [24,25]. Matrigel-based models are relatively easily

 doi:10.20944/preprints202511.0438.v1

established, as Matrigel contains a growth factor cocktail that can support most primary cell types, including salivary epithelial and stromal cells [5,6,8,11,13,14]. However, its batch-to-batch variability, sarcoma tumor-derived and ill-defined composition can skew study results [26,27] and make it unsuitable for clinical translation. Several hydrogel-based *in vitro* salivary gland models have been developed to attempt to replace Matrigel-based cultures [16,17]; however, in these systems, the bulk hydrogel completely encapsulates salivary epithelial and stromal cells, failing to mimic the porous native extracellular matrix (ECM) architecture, and inadequately mimicking salivary ECM mechanical properties and cell-ECM interactions. Scaffold-free organoid models avoid the complexity of incorporating physiologically relevant biomaterial scaffolds but tend to mimic the early gland developmental stages rather than the complexity of adult gland cell-cell interactions and cell-ECM interactions [28]. While organoids are good candidates to study developmental disorders and cancers, they may not mimic other adult human pathologies [28,29]. Thus, there is a need to develop physiologically relevant *in vitro* models that comprehensively mimic the native 3D cell organization, cell–cell communication, cell–ECM interactions, and cell phenotypes, for translational preclinical research. Such functional 3D tissue models could also serve as platforms for regenerative, implantable therapies.

We previously developed 3D cryoelectrospun scaffolds (CES) with fibrous (CES-F) and honeycomb-like (CES-H) topographies and showed that CES-H mimics the porosity, pore size, and viscoelasticity of native salivary ECM [30,31]. CES-H supported the maintenance of mesenchymal stromal cells (MSC), preserving their innate phenotype [31,32]. MSCs on CES-H exerted therapeutic, anti-fibrotic effects on fibrotic myofibroblasts in a preclinical *in vitro* model [32], ameliorating fibrosis, the underlying pathology in salivary gland hypofunction. Additionally, we demonstrated that MSC-CES-H implants were biocompatible, eliciting neither inflammatory nor fibrotic effects in mice [32].

In this study, we address some of the limitations of current *in vitro* salivary tissue models by applying CES for salivary tissue engineering. We explored whether CES can support salivary epithelial monoculture and epithelial-stromal coculture. *In vivo*, epithelial cells reside on fibrous basement membranes, which regulate their function and phenotype. *In vitro*, epithelial cells are difficult to grow on tissue culture plastic due to limited expansion potential, senescence, and transdifferentiation, necessitating growth in Matrigel and/or with special media formulations containing specific growth factors or small molecules [33–35]. Here, we evaluate the role of scaffold topography on epithelial cell phenotype and cell organization in 3D salivary epithelial cultures by comparing honeycomb-like CES-H with densely packed electrospun nanofibers (NF) and fibrous CES-F. Since stromal cells serve as a key player in regulating epithelial cell health in the salivary gland and *in vitro* salivary gland culture systems [36,37], we also evaluate the role of stromal fibroblast cells in combination with scaffold topography (CES-F vs. CES-H) in regulating epithelial phenotype and 3D epithelial and stromal cell organization. Overall, we assess the potential of CES to bioengineer 3D salivary epithelial-stromal cocultures towards functional salivary tissue engineering for preclinical research and regenerative medicine strategies.

2. Results

2.1. Characterization of Scaffold Topography Prior to Cell Seeding

Scaffold topography critically influences cell attachment and the number of activated adhesion sites, regulating downstream mechanotransduction pathways that shape cell phenotype. Epithelial cells typically reside on densely packed nanofibrous basement membranes with kPa-MPa stiffness [38,39], whereas stromal cells reside in loosely packed, viscoelastic, reticulated, porous matrices with sub-kPa to low kPa stiffness [40–42]. We hypothesized that 3D matrices integrating features of both basement membrane and stromal ECM would facilitate the growth of 3D epithelial–stromal cocultures. To test this hypothesis, we fabricated electrospun nanofiber (NF) mats and cryoelectrospun scaffolds with fibrous (CES-F) or honeycomb (CES-H) topography from elastin–alginate biopolymers to mimic the compliant nature of stromal ECM and/or fibrous topography of epithelial basement membranes as previously described [30,31,43]. NF mats were fabricated to

 doi:10.20944/preprints202511.0438.v1

resemble the densely packed, fibrous nature of basement membranes. CES-F were designed to mirror the fibrous topography of basement membranes and loosely packed nature of stromal ECM; whereas, CES-H were designed to resemble the porous and loosely packed nature of stromal ECM. Scanning electron microscopy (SEM) revealed that nanofiber (NF) mats were composed of densely packed, ~200 nm ± 5 nm-diameter nanofibers with < 2 μm pores (Table 1), forming a 2.5D mat (Figure 1A, D). CES-F showed loosely packed ~178 nm ± 80 nm-diameter nanofibers with < 5 μm pores (Table 1), forming a taller 3D structure (Figure 1B, E). In contrast, CES-H displayed a honeycomb-like, reticulated topography (Figure 1C, F, G), with larger backbones (~4.72 ± 3.86 μm width) and pores (~15-25 μm diameter) (Table 1), forming a 3D scaffold similar in height to CES-F (Figure 1B, C).

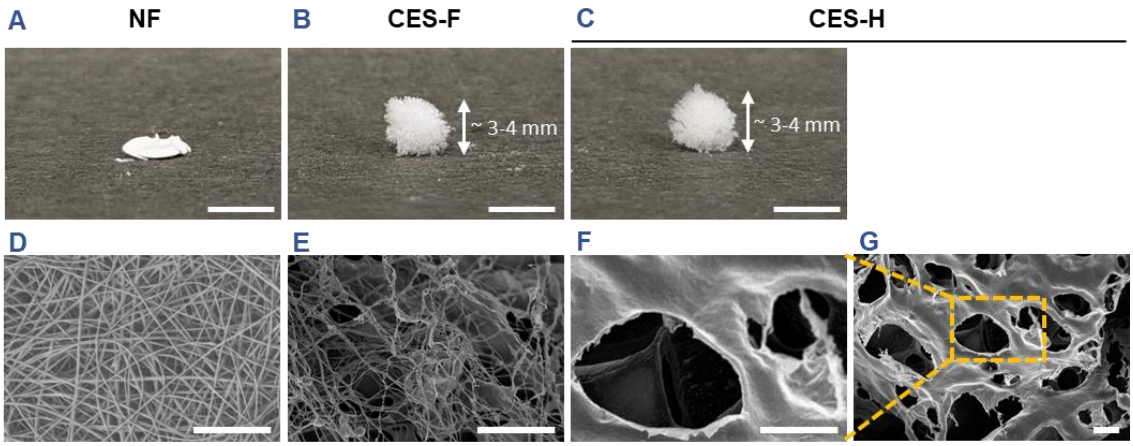

Figure 1. Benchtop photos and SEM images depicting the scaffold dimensions and topography. (A, D) Electrospun nanofibers (NF). (B, E) Cryoelectrospun scaffolds with fibrous topography (CES-F). (C, F, G) Cryoelectrospun scaffolds with honeycomb topography (CES-H). (A – C) Benchtop photos. Scale bar = 5 mm. (D – G) SEM images. Scale bar = 10 μm.

Table 1. Summary of scaffold topographical features.

Scaffold type	Minimum fiber diameter or backbone width	Maximum fiber diameter or backbone width	Average fiber diameter or backbone width	Pore size
NF	108 nm	329 nm	200 nm ± 54 nm	< 2 μm
CES-F	62 nm	363 nm	178 nm ± 80 nm	< 5 μm
CES-H	980 nm	28 μm	4.72 ± 3.86 μm	15-25 μm

2.2. Cryoelectrospun Scaffolds with Honeycomb and Fibrous Topography Promote Clustered Salivary Epithelial Cell Growth

Cell–cell adhesion and morphology are key determinants of epithelial phenotype and function [44]. To assess how scaffold topography affects epithelial attachment and clustering, SIMS cells, an established submandibular salivary gland ductal epithelial line [45], were cultured on NF, CES-F, and CES-H scaffolds. After 1 day of culture, the SIMS cells on scaffolds were imaged using SEM. On NF mats, epithelial cells remained rounded (Figure 2A), whereas on CES-F and CES-H scaffolds they exhibited distinct cell bodies and formed cell clusters (Figures 2B, C).

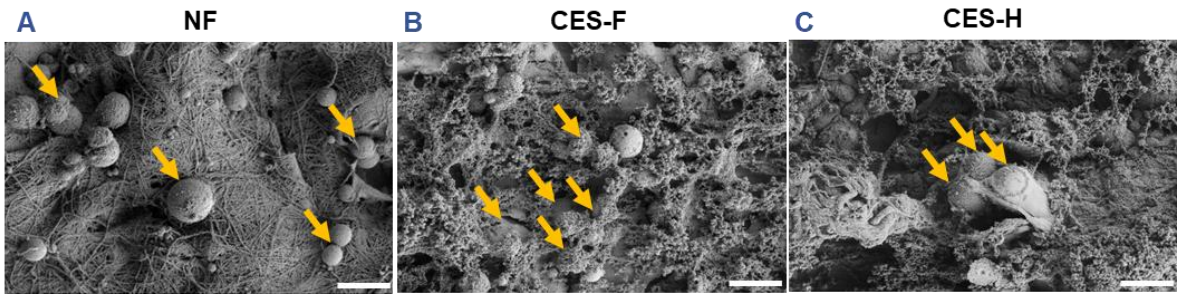

 doi:10.20944/preprints202511.0438.v1

Figure 2. Effects of scaffold topography on SIMS epithelial cell morphology and clustering. SEM images showed that SIMS epithelial cells remained isolated and rounded on conventionally electrospun nanofibers (NF) (A) and formed cell clusters on cryoelectrospun scaffolds with fibrous topography (CES-F) (B) and honeycomb topography (CES-H) (C) after 1 day in culture. Arrows denote cells. Scale bar = 25 μm.

2.3. Cryoelectrospun Scaffolds with Honeycomb Topography Enable Deep Penetration of 3D Salivary Epithelial Cell Clusters and Distinct 3D Epithelial-Stromal Organization in Cocultures

3D culture enhances expression of genes linked to epithelial function, in comparison to 2D culture [46]. Stromal–epithelial interactions further regulate epithelial phenotype and function [36,47,48]. To assess how scaffold architecture affects 3D growth and penetration of epithelial cell clusters and maintenance of epithelial cell morphology, SIMS epithelial cells (monoculture) were cultured on NF, CES-F, and CES-H scaffolds for 4 days (Figure 3A). To examine scaffold-topography-dependent stromal–epithelial organization, SIMS cells were cocultured with NIH 3T3 fibroblasts, a stromal model [49], on each scaffold type. We anticipated that appropriate topography would result in distinct 3D cell clusters, similar to stromal and parenchymal compartmentalization observed *in vivo* [50]. NIH 3T3 fibroblasts were seeded first and allowed to expand for 2 days to act as stromal support for SIMS cells, which were subsequently seeded and cocultured with the fibroblasts for 4 additional days (Figure 3B).

SIMS cells were identified by immunostaining for intercellular epithelial junction markers, E-cadherin and Zona occludin-1 (ZO-1) [51], while NIH 3T3 cells were identified by immunostaining for vimentin, a mesenchymal phenotype marker [52]. 4′,6-diamidino-2-phenylindole (DAPI) was used for nuclear staining for both cell types. NF mats showed poor cell attachment in both SIMS monocultures and SIMS–NIH 3T3 cocultures (Figures 3A, B, left panels). On CES-F, SIMS monocultures formed thin epithelial sheets (Figure 3A, middle panel), whereas on CES-H, they penetrated the scaffold, forming deep 3D clusters (Figure 3A, right panel). In cocultures, CES-F showed random cell attachment (Figure 3B, middle panel), whereas CES-H supported the self-organization of epithelial and stromal cells into distinct clusters (Figure 3B, right panel).

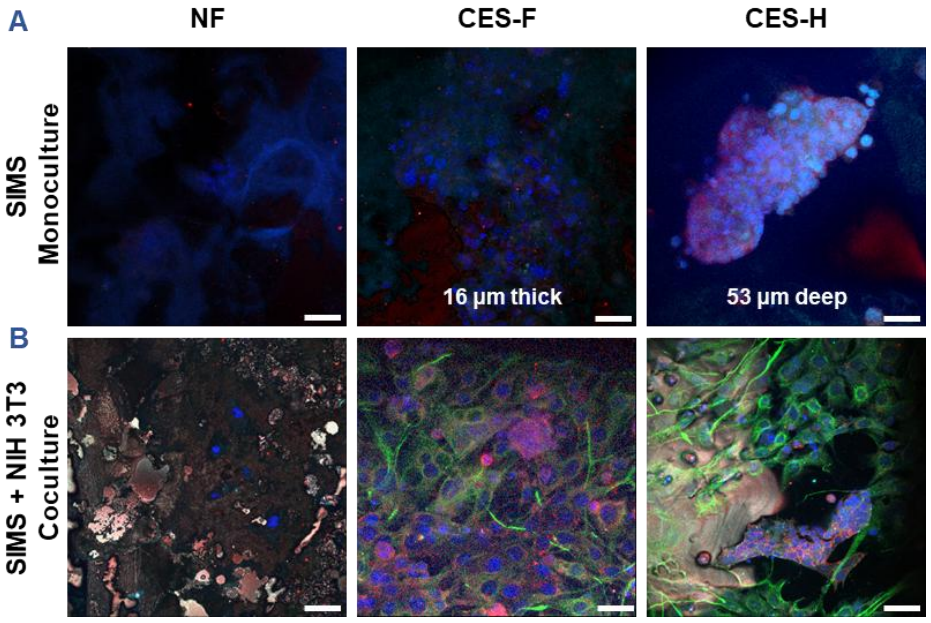

Figure 3. Confocal images showing effects of scaffold topography on 3D organization of SIMS epithelial cells in monoculture and coculture with NIH 3T3 fibroblasts. (A) SIMS monoculture on scaffolds. (B) SIMS epithelial cells cocultured with NIH 3T3 fibroblasts on scaffolds. Cells grown on NF mats (left panel), CES with fibrous topography (CES-F) (middle panel), and CES with honeycomb topography (CES-H) (right panel) were immunostained with epithelial junction markers (E-cadherin in red and ZO-1 in cyan) and mesenchymal marker (vimentin in green) along with DAPI-stained nuclei (in bluish purple) on day 4. SIMS monocultures penetrated

 doi:10.20944/preprints202511.0438.v1

CES-H, forming deep 3D clusters (top right) whereas they remained on the surface of CES-F, forming thin cell sheets (top middle). SIMS and NIH 3T3 cocultures showed distinct organization of cells into separate clusters on CES-H (bottom right), reminiscent of tissues *in vivo*, but remained random on CES-F (bottom middle). Very few cells attached and grew on NF; blue fluorescence observed is primarily autofluorescence (left panels). Scale bar = 25 μm.

2.4. Stromal Cells on Cryoelectrospun Scaffolds with Honeycomb Topography Facilitate Phenotypic Maintenance of Salivary Epithelial Cells

Since CES-H promoted stromal–epithelial organization into distinct 3D clusters (Figure 3B, right panel), we examined whether stromal cells influence epithelial phenotype over 1, 4, and 7 days of culture. SIMS epithelial cells were cultured alone or cocultured with NIH 3T3 fibroblasts on CES-H scaffolds. Using confocal microscopy, epithelial phenotype was assessed by E-cadherin and ZO-1 expression and localization, as E-cadherin assembled at cell membranes is indicative of formation of adherens junctions and ZO-1 of tight junctions between epithelial cells [51]. Stromal cells were identified by vimentin immunostaining; all nuclei were counterstained with DAPI. In monoculture, SIMS cells on CES-H showed expression of E-cadherin by day 4 but little ZO-1 (Figure 4A). In coculture with NIH 3T3 cells on CES-H, SIMS cells formed robust 3D clusters with strong membrane localization of both epithelial markers from day 4 to 7 (Figure 4B). These findings demonstrate that stromal cells cultured on CES-H play a critical role in enhancing epithelial cell phenotype and polarization compared to epithelial monocultures.

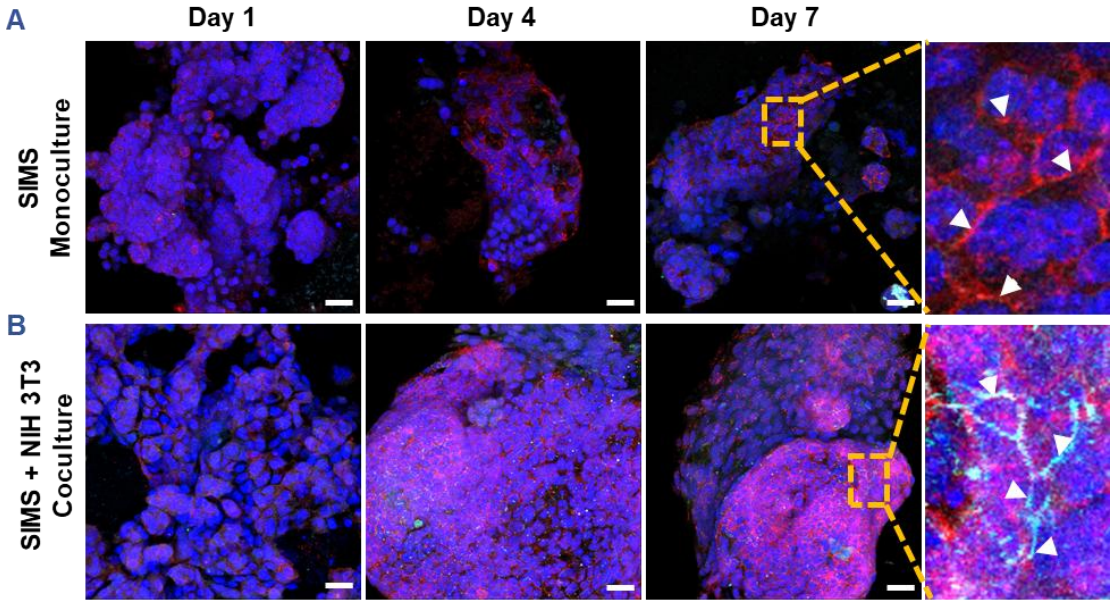

Figure 4. Confocal images showing effects of stromal support on epithelial cell phenotype on cryoelectrospun scaffolds with honeycomb topography. (A) SIMS epithelial monoculture on CES-H demonstrated 3D cell growth with membrane-localized expression of E-cadherin but not ZO-1. (B) Coculture of SIMS epithelial cells with NIH 3T3 fibroblasts promotes membrane-localized expression of both epithelial markers, ZO-1 and E-cadherin. Monocultures of SIMS salivary epithelial cells were immunostained for E-cadherin (red) and ZO-1 (cyan). Cocultures of SIMS epithelial cells and NIH 3T3 fibroblasts were stained for stained for vimentin (green), E-cadherin (red) and ZO-1 (cyan) along with DAPI stain of nuclei (bluish purple). (Left three panels) Cells cultured on CES-H on days 1, 4, and 7. (Right panel) Enlarged view of cells cultured on CES-H on day 7. Arrowheads point to membrane-localized expression of E-cadherin and/or ZO-1. Scale bar = 25 μm.

3. Discussion

Matrix topography, architecture, composition and mechanical properties govern cell–matrix interactions and, together with cell–cell communication, regulate cell function in health and disease

 doi:10.20944/preprints202511.0438.v1

[40,53–55]. Replicating these cues is essential for developing physiologically relevant tissues for preclinical research or regenerative therapy. *In vitro* cell culture systems, aiming to recapitulate the epithelial lining or epithelial-stromal interface, typically grow epithelial cells on dense basement membrane-like matrices or encapsulate epithelial and stromal cells in hydrogels [56–60]. While stiff nanofiber mats composed of water-insoluble biomaterials support robust epithelial cell growth [56–58,61], we hypothesized that matrices incorporating both epithelial and stromal ECM properties would better support epithelial–stromal cocultures. We therefore compared three scaffold types representing distinct epithelial and/or stromal ECM properties.

Densely packed electrospun nanofibers (NF) fabricated from an elastin-alginate solution resembled the structural architecture of epithelial basement membranes, and the compliant nature of stromal ECM but poorly supported epithelial cell attachment in both monocultures and epithelial-stromal cocultures (Figures 2A, 3A-B left panels). This result was consistent with our prior work with NIH 3T3 stromal cells, where the alginate in these NF scaffolds swelled to form a unified hydrogel layer [30], limiting cell adhesion and viability. Therefore, densely packed nanofibers may be suitable for epithelial culture, only when composed of insoluble, stiff biomaterials that preserve the nanofibrous topography upon hydration.

Loosely packed cryoelectrospun scaffolds (CES-F) combining the fibrous nature of basement membranes, and the loosely packed, compliant 3D structure of stromal ECM supported epithelial cell attachment and morphology (Figures 2B, 3A-B middle panels). Unlike NF mats, CES-F retained topography upon hydration, permitting cell adhesion and clustering. However, its fibrous mesh limited vertical cell penetration, leading to horizontal 1 to 3-layer thick cell sheets in both mono- and cocultures (Figure 3A-B middle panels), and a random mix of epithelial and stromal cells in cocultures rather than distinct 3D clusters. Thus, CES-F supports epithelial attachment but not 3D epithelial–stromal organization.

Cryoelectrospun scaffolds with a honeycomb-like, reticulated topography (CES-H) supported epithelial attachment, clustering, and at least 50 μm-deep penetration (Figures 2C, 3A right panel). However, CES-H alone only maintained E-cadherin expression and localization, and not ZO-1 expression (Figure 4A), possibly because CES-H does not mimic the structure or complex composition of epithelial basement membranes. Stromal coculture on CES-H restored membrane-localized E-cadherin and ZO-1 expression (Figure 4B) in SIMS cells, highlighting the necessity of stromal support for maintaining epithelial phenotypes on CES-H. We previously demonstrated that CES-H recapitulates the viscoelastic and topographical properties of native salivary ECM [30] and supports stromal cells while suppressing fibrotic differentiation [32]. Furthermore, we showed that CES-H suppressed the fibrotic phenotype in myofibroblasts *in vitro* [32]. The physical and mechanical properties of CES-H might be best suited for optimal stromal culture, which likely enabled NIH 3T3 fibroblasts to sustain the epithelial phenotype of SIMS cells through paracrine signaling or ECM deposition. Stromal cells regulate salivary epithelial function via growth factors (e.g., fibroblast growth factors, bone morphogenetic proteins and macrophage colony stimulating factor), ECM modulation and direct epithelial–stromal interactions [36,37,62–65]. However, the specific mechanisms by which stromal cells on CES-H promote the epithelial phenotype remain to be investigated. CES-H also promoted the most physiologically relevant 3D organization of stromal and epithelial clusters (Figure 3A–B middle vs. right panels). The larger (~15–25 μm) pores likely enabled deeper penetration and spatial segregation of clusters, mimicking native stromal–parenchymal architecture.

These foundational studies demonstrate that matrices that support stromal cell growth and phenotype maintenance might best facilitate healthy stromal–epithelial cocultures. While densely packed nanofiber mats or loosely packed fibrous meshes fabricated with stiff insoluble biomaterials (e.g., collagen, laminin) may enable cell attachment and growth of epithelial and stromal cells, they risk inducing stromal fibrosis and thereby, epithelial to mesenchymal transition [66–69]. Such stiff scaffolds may be better suited for modeling diseased or fibrotic tissue, but not healthy tissue.

 doi:10.20944/preprints202511.0438.v1

Further work is necessary to validate the utility of CES-H to support more physiologically relevant parenchymal-stromal cocultures, using primary or stem cell-derived epithelial and stromal cells, to evaluate acinar differentiation and secretory function, as softer matrices promote salivary morphogenesis [70]. Given the soft ECM-like properties of CES-H, it may also be adaptable for stromal–parenchymal cocultures of other soft tissues such as lung, liver, and pancreas, building on these foundational studies.

4. Conclusions

Cryoelectrospun scaffolds with honeycomb topography supported 3D growth and organization of SIMS epithelial cells in both monocultures and cocultures with NIH 3T3 fibroblasts. Cells penetrated the CES-H scaffolds and self-organized into tissue-like structures with characteristic epithelial-like organization. These findings provide a foundation for future applications of CES-H scaffolds for *in vitro* organ modeling and *in vivo* soft tissue regeneration.

5. Materials and Methods

5.1. Materials

Scaffolds were fabricated using soluble bovine neck elastin (ES12; Elastin Products Co., Owensville, MI), alginate, and 400 kD polyethylene oxide (PEG-400kD) from Sigma-Aldrich (St. Louis, MO). Scaffold-crosslinking reagents were N-hydroxysuccinimide (NHS; Thermo Fisher Scientific, Waltham, MA), ethyl dimethylaminopropyl carbodiimide (EDC), and calcium chloride dihydrate (both from Sigma-Aldrich). Cell culture reagents were high-glucose Dulbecco's Modified Eagle's Medium (DMEM), heat-inactivated fetal bovine serum (FBS), Penicillin-Streptomycin (10,000 U/mL penicillin and 10,000 µg/mL streptomycin) all from Thermo Fisher Scientific, or Antibiotic-Antimycotic Solution (10,000 U/mL penicillin, 10,000 µg/mL streptomycin and 25 µg/mL amphotericin B; R&D Systems, Minneapolis, Minnesota). Multi-well, cell culture plates were coated with the ultra-low adhesion polymer Lipidure (Amsbio; Cambridge, MA). For scanning electron microscopy (SEM) sample preparation, glutaraldehyde, sucrose, phosphate buffer, and hexamethyldisilazane (HMDS) were obtained from Sigma-Aldrich, and ethanol was obtained from Decon Labs (King of Prussia, PA). Primary antibodies used for immunocytochemistry analysis included mouse anti-vimentin (µ-chain specific; clone LN-6; Cat. No. V2258; Sigma-Aldrich), rabbit anti-ZO-1 (Cat. No. 402200; Thermo Fisher Scientific), and mouse anti-E-cadherin (Cat. No. 610182; BD Biosciences, San Jose, CA). Secondary antibodies (Jackson ImmunoResearch Laboratories, West Grove, PA) used were donkey anti-rabbit Cyanine Cy3 AffiniPure IgG (Cat. No. 711-165-152) for ZO-1, Alexa Fluor-488 AffiniPure $F(ab')_2$ Fragment IgM (Cat. No. 715-546-020) for vimentin, and donkey anti-rabbit Alexa Fluor-647 AffiniPure F(ab')2 fragment (Cat. No. 715-606-150) for E-cadherin. Other reagents used for immunocytochemistry analysis included paraformaldehyde, Tween 20, bovine serum albumin, glutaraldehyde, Triton X-100, sodium chloride, and DAPI (all from Sigma-Aldrich), normal donkey serum (Cat. No. 017-000-121; Jackson ImmunoResearch Laboratories), and Fluoro-Gel mounting medium (Electron Microscopy Sciences; Hatfield, PA).

5.2. Scaffold Fabrication and Modification

Cryoelectrospinning was performed using 1% elastin, 1.5% alginate, and 3% PEG-400kD in deionized water as previously described [30]. The solution was electrospun at 17 kV (needle voltage), 10 µL/min (flow rate), through a 25G needle with a 15 cm tip-to-collector distance onto a custom probe-array collector maintained at −15 to −20 °C for 1 h. The entire setup was maintained at relative humidity (RH) > 35%, and air temperature was modulated to < 2 °C to fabricate CES-H and > 2 °C to fabricate CES-F. After cryoelectrospinning, the collector with the scaffolds was immediately lyophilized (FreeZone, Labconco, Kansas City, MI) for 2–3 h.

Lyophilized elastin-alginate-PEG scaffolds were individually crosslinked in a 96-well plate using EDC and NHS (1.48 mg EDC + 1.78 mg NHS per 100 µL 95% ethanol per scaffold) to covalently link elastin and alginate chains. PEG-400kD does not have pendant groups that can be crosslinked

 doi:10.20944/preprints202511.0438.v1

and dissolves away in water in the subsequent wash steps. Scaffolds were rocked at 45 rpm for 2 h, then washed sequentially in 95%, 70%, 50%, and 0% ethanol containing 1.5% $CaCl_2$ for 15 min each to remove residual EDC and NHS and ionically crosslink alginate chains. Finally, scaffolds were frozen at −80 °C and lyophilized for 4 h.

Elastin-alginate nanofiber (NF) mats were fabricated by conventional electrospinning of the same 1% elastin/1.5% alginate/3% PEG-400kD solution, using identical parameters except that the collector was maintained at room temperature and RH < 35% with dehumidified air.

All scaffolds were UV-sterilized, soaked in 70% ethanol + 50 mM $CaCl_2$ for 30 min, rinsed with 0.9% NaCl + 50 mM $CaCl_2$ for 10 min, and hydrated overnight in culture medium (10% FBS, 5% Antibiotic-Antimycotic Solution, 50 mM $CaCl_2$) prior to cell seeding.

5.3. Scanning Electron Microscopy (SEM)

5.3.1. SEM of Scaffolds

Electrospun NF mats and lyophilized cryoelectrospun CES-H and CES-F scaffolds were prepared for SEM imaging before crosslinking to prevent hydration. Scaffolds were sputter-coated with iridium-palladium and imaged using a Zeiss Leo 1550 field emission scanning electron microscope (Zeiss Leo Electron Microscopy Ltd., Cambridge, UK).

5.3.2. SEM of Scaffolds with Cells

Scaffolds seeded with cells were fixed with 4% paraformaldehyde-0.25% glutaraldehyde in 5% (w/v) sucrose and 0.6X phosphate buffered saline (PBS) for 20 minutes, followed by 3% glutaraldehyde in 0.1 M sucrose-0.1M phosphate buffer (pH 7.4) for 2 hours. Fixed samples were washed three times (10 minutes each) in 0.1 M sucrose-0.1M phosphate buffer, dehydrated through graded ethanol (25%, 50%, 70%, 80%, 95%, 100%, and 100%) for 15 minutes per step, and chemically dried in ethanol/HMDS mixtures (3:1, 1:1, and 1:3 ethanol: HMDS) for 15 min each, followed by three rinses in 100% HMDS (15 min each). Samples were air-dried overnight, sputter-coated with iridium-palladium and imaged using a Zeiss Leo 1550 field emission SEM.

5.4. Image Analysis of Scaffold Topographical Features

SEM images of NF, CES-H and CES-F scaffolds were analyzed in ImageJ to quantify fiber diameter or backbone width and pore size. Measurements were taken from 50–100 features per image using the 'Analyze > Measure' tool.

5.5. Cell Culture

Mouse embryonic NIH 3T3 fibroblasts [49] (passage 12-17) and SIMS mouse submandibular salivary gland ductal epithelial cells were cultured in DMEM containing 10% FBS and 1% penicillin-streptomycin at 37 °C, in a 5% CO_2 humidified incubator. NIH 3T3 fibroblasts were subcultured on day 3 or 4 at 70-80% confluence and SIMS cells every 2 or 3 days at 80-95% confluence.

5.6. Cell Culture on Scaffolds

NIH 3T3 fibroblasts and SIMS cells were seeded at 75,000 cells/scaffold in 25 µL DMEM (10% FBS, 1% penicillin-streptomycin, and 25 mM $CaCl_2$) in ultra-low adhesion, Lipidure polymer-coated, round-bottom, 96-well plates. Plates were incubated on a rotary shaker at 30 rpm for 2 hours to promote cell attachment to the scaffolds. 25 mM $CaCl_2$ supplementation was used to prevent rapid disintegration of the scaffold, a concentration at which cell health was not negatively impacted [17,30,32]. After 2 hours, 175 µL of fresh medium was added to each well and rotary shaking continued for an additional 22 hours to increase the cell attachment efficiency. After 24 hours, constructs were transferred to Lipidure-coated 24-well plates with 200 µL fresh medium to enhance oxygen transfer and cell viability [30]. Cells were maintained in static culture for 7 days with daily partial media changes (100 µL removed, 150 µL added) to retain conditioned medium while replenishing nutrients and compensating for evaporative losses.

 doi:10.20944/preprints202511.0438.v1

For SIMS/NIH 3T3 cocultures, 50,000 NIH 3T3 cells were first seeded on the scaffold as described above and grown for 2 days to provide stromal support before adding 50,000 SIMS cells in the same manner.

5.7. Immunochemistry Analysis and Confocal Imaging of Cell-Scaffold Constructs

Cell-scaffold constructs were fixed in 4% paraformaldehyde-0.25% glutaraldehyde in 5% (w/v) sucrose, 0.6X PBS for 15 minutes, permeabilized with 0.1% Triton X-100 in 1× PBS for 15 min, blocked with 20% donkey serum-3% bovine serum albumin in wash buffer (0.9% NaCl-50mM $CaCl_2$ in deionized water) for 2 hours at room temperature. Samples were incubated overnight at 4 °C with primary antibodies, mouse μ-chain specific anti-vimentin (clone LN-6), rabbit polyclonal anti-ZO-1 and mouse monoclonal anti-E-cadherin followed by 2-hour, room-temperature incubation with DAPI and secondary antibodies, donkey anti-rabbit Cyanine Cy3 (to reveal ZO-1), donkey anti-mouse IgM Alexa Fluor-488 (to reveal vimentin), and donkey anti-mouse IgG Alexa Fluor-647 (to reveal E-cadherin). NIH 3T3 fibroblasts were immunostained for vimentin and SIMS epithelial cells were stained for E-cadherin and ZO-1. All samples were counterstained with DAPI and mounted in Fluoro-Gel mounting medium for confocal imaging using a Leica SP5 confocal laser scanning microscope (Leica Microsystems, Mannheim, Germany).

6. Patents

Pujhitha Ramesh, James Castracane, Melinda Larsen, Susan Sharfstein, and Yubing Xie have pending patent applications (US Patent App. 17/558,543 and 18/108,395) related to this work.

Author Contributions: P.R. contributed to conceptualization, methodology, investigation, data curation, analysis, visualization, validation, and writing, reviewing and submission of the manuscript. M.L., Y.X., and S.S. provided funding, supervision, conceptualization, analysis, project administration and reviewed the manuscript. J.C. and D.N. contributed to the conceptualization of the work. All authors have read and agreed to the published version of the manuscript.

Funding: This research was funded by the National Institute of Health (NIH) National Institute of Dental & Craniofacial Research (NIDCR) under the grant number DE027953 (M.L.).

Ethical Statement: The NIH 3T3 cell line was obtained from the ATCC, and the SIMS cell line was a gift from Dr. Daniel Malamud.

Data Availability Statement: The original contributions presented in the study are included in the article; further inquiries can be directed to the corresponding authors.

Acknowledgments: We would like to thank Mr. Adam Koplas and Mr. Zachary Hanchon for their assistance in scaffold preparation and Dr. Nicholas Moskwa for scientific discussions.

Conflicts of Interest: Pujhitha Ramesh, James Castracane, Melinda Larsen, Susan T. Sharfstein, and Yubing Xie are co-inventors on pending patent applications (US Patent App. 17/558,543 and 18/108,395) related to this work. The funders had no role in the design of the study; in the collection, analyses, or interpretation of data; in the writing of the manuscript; or in the decision to publish the results.

Abbreviations

The following abbreviations are used in this manuscript:

CES	Elastin-alginate cryoelectrospun scaffolds
CES-F	Elastin-alginate cryoelectrospun scaffolds with fibrous topography
CES-H	Elastin-alginate cryoelectrospun scaffolds with honeycomb topography
DAPI	Diamidino-2-phenylindole
DMEM	Dulbecco's modified eagle medium
ECM	Extracellular matrix
FBS	Fetal bovine serum

 doi:10.20944/preprints202511.0438.v1

HMDS	Hexamethyldisilazane
MSC	Mesenchymal stromal cells
NF	Conventionally electrospun nanofibers
PBS	Phosphate buffered saline
PEG	Poly(ethylene glycol)
SEM	Scanning electron microscopy
ZO-1	Zona occludin-1

References

1. Krishnamurthy, S.; Vasudeva, S.B.; Vijayasarathy, S. Salivary Gland Disorders: A Comprehensive Review. *World Journal of Stomatology* **2015**, *4*, 56–71, doi:10.5321/WJS.V4.I2.56.
2. Vistoso Monreal, A.; Polonsky, G.; Shiboski, C.; Sankar, V.; Villa, A. Salivary Gland Dysfunction Secondary to Cancer Treatment. *Frontiers in Oral Health* **2022**, *3*, 907778, doi:10.3389/FROH.2022.907778.
3. Almansoori, A.A.; Kim, B.; Lee, J.H.; Tran, S.D. Tissue Engineering of Oral Mucosa and Salivary Gland: Disease Modeling and Clinical Applications. *Micromachines (Basel)* **2020**, *11*, 1–13, doi:10.3390/mi11121066.
4. Nelson, J.; Manzella, K.; Baker, O.J. Current Cell Models for Bioengineering a Salivary Gland: A Mini-Review of Emerging Technologies. *Oral Dis* **2013**, *19*, 236–244, doi:10.1111/j.1601-0825.2012.01958.x.
5. Rahman, Z.A. The Development of in Vitro Models of Human Salivary Glands. *Doctoral thesis* **2018**.
6. Tanaka, J.; Mishima, K. In Vitro Three-Dimensional Culture Systems of Salivary Glands. *Pathol Int* **2020**, *70*, 493–501, doi:10.1111/pin.12947.
7. Su, X.; Fang, D.; Liu, Y.; Ramamoorthi, M.; Zeitouni, A.; Chen, W.; Tran, S.D. Three-Dimensional Organotypic Culture of Human Salivary Glands: The Slice Culture Model. *Oral Dis* **2016**, *22*, 639–648, doi:10.1111/odi.12508.
8. Burghartz, M.; Lennartz, S.; Schweinlin, M.; Hagen, R.; Kleinsasser, N.; Hackenberg, S.; Steußloff, G.; Scherzad, A.; Radeloff, K.; Ginzkey, C.; et al. Development of Human Salivary Gland-Like Tissue In Vitro. *Tissue Eng Part A* **2018**, *24*, 301–309, doi:10.1089/ten.tea.2016.0466.
9. Rose, S.C.; Larsen, M.; Xie, Y.; Sharfstein, S.T. Salivary Gland Bioengineering. *Bioengineering* **2024**, *11*, doi:10.3390/bioengineering11010028.
10. Phan, T. V.; Oo, Y.; Ahmed, K.; Rodboon, T.; Rosa, V.; Yodmuang, S.; Ferreira, J.N. Salivary Gland Regeneration: From Salivary Gland Stem Cells to Three-Dimensional Bioprinting. *SLAS Technol* **2023**, *28*, 199–209, doi:10.1016/j.slast.2023.03.004.
11. Hosseini, Z.F.; Nelson, D.A.; Moskwa, N.; Larsen, M. Generating Embryonic Salivary Gland Organoids. *Curr Protoc Cell Biol* **2019**, *83*, e76, doi:10.1002/CPCB.76.
12. Hajiabbas, M.; D'Agostino, C.; Simińska-Stanny, J.; Tran, S.D.; Shavandi, A.; Delporte, C. Bioengineering in Salivary Gland Regeneration. *J Biomed Sci* **2022**, *29*, 1–24, doi:10.1186/s12929-022-00819-w.
13. Kim, D.; Yoon, Y.J.; Choi, D.; Kim, J.; Lim, J.Y. 3D Organoid Culture From Adult Salivary Gland Tissues as an Ex Vivo Modeling of Salivary Gland Morphogenesis. *Front Cell Dev Biol* **2021**, *9*, 1–11, doi:10.3389/fcell.2021.698292.
14. Sui, Y.; Zhang, S.; Li, Y.; Zhang, X.; Hu, W.; Feng, Y.; Xiong, J.; Zhang, Y.; Wei, S. Generation of Functional Salivary Gland Tissue from Human Submandibular Gland Stem/Progenitor Cells. *Stem Cell Res Ther* **2020**, *11*, 1–13, doi:10.1186/s13287-020-01628-4.
15. Zhao, C.; Meng, C.; Cui, N.; Sha, J.; Sun, L.; Zhu, D. Organoid Models for Salivary Gland Biology and Regenerative Medicine. *Stem Cells Int* **2021**, *2021*, doi:10.1155/2021/9922597.
16. Ozdemir, T.; Fowler, E.W.; Hao, Y.; Ravikrishnan, A.; Harrington, D.A.; Witt, R.L.; Farach-Carson, M.C.; Pradhan-Bhatt, S.; Jia, X. Biomaterials-Based Strategies for Salivary Gland Tissue Regeneration. *Biomater Sci* **2016**, *4*, 592–604, doi:10.1039/c5bm00358j.
17. Jorgensen, M.; Ramesh, P.; Toro, M.; Evans, E.; Moskwa, N.; Zhang, X.; Sharfstein, S.T.; Larsen, M.; Xie, Y. Alginate Hydrogel Microtubes for Salivary Gland Cell Organization and Cavitation. *Bioengineering* **2022**, *9*, doi:10.3390/bioengineering9010038.
18. Piraino, L.R.; Benoit, D.S.W.; Delouise, L.A. Salivary Gland Tissue Engineering Approaches: State of the Art and Future Directions. *Cells* **2021**, *10*, doi:10.3390/cells10071723.

 doi:10.20944/preprints202511.0438.v1

19. Pillai, S.; Munguia-Lopez, J.G.; Tran, S.D. Bioengineered Salivary Gland Microtissues—A Review of 3D Cellular Models and Their Applications. *ACS Appl Bio Mater* **2024**, *7*, 2620–2636, doi:10.1021/acsabm.4c00028.
20. Shin, H.S.; Hong, H.J.; Koh, W.G.; Lim, J.Y. Organotypic 3D Culture in Nanoscaffold Microwells Supports Salivary Gland Stem-Cell-Based Organization. *ACS Biomater Sci Eng* **2018**, *4*, 4311–4320, doi:10.1021/acsbiomaterials.8b00894.
21. Kim, J.Y.; An, C.H.; Kim, J.Y.; Jung, J.K. Experimental Animal Model Systems for Understanding Salivary Secretory Disorders. *International Journal of Molecular Sciences 2020, Vol. 21, Page 8423* **2020**, *21*, 8423, doi:10.3390/IJMS21228423.
22. Gao, Y.; Chen, Y.; Zhang, Z.; Yu, X.; Zheng, J. Recent Advances in Mouse Models of Sjögren's Syndrome. *Front Immunol* **2020**, *11*, 471903, doi:10.3389/FIMMU.2020.01158/XML.
23. Gluck, C.; Min, S.; Oyelakin, A.; Smalley, K.; Sinha, S.; Romano, R.A. RNA-Seq Based Transcriptomic Map Reveals New Insights into Mouse Salivary Gland Development and Maturation. *BMC Genomics* **2016**, *17*, 1–18, doi:10.1186/S12864-016-3228-7/FIGURES/7.
24. Maruyama, C.L.; Monroe, M.M.; Hunt, J.P.; Buchmann, L.; Baker, O.J. Comparing Human and Mouse Salivary Glands: A Practice Guide for Salivary Researchers. *Oral Dis* **2018**, *25*, 403, doi:10.1111/ODI.12840.
25. Frangogiannis, N.G. Why Animal Model Studies Are Lost in Translation. *The journal of cardiovascular aging* **2022**, *2*, 22, doi:10.20517/JCA.2022.10.
26. Aisenbrey, E.A.; Murphy, W.L. Synthetic Alternatives to Matrigel. *Nat Rev Mater* **2020**, *5*, 539, doi:10.1038/S41578-020-0199-8.
27. Revilla, S.A.; Cutilli, A.; Cambiaso, E.; Rockx-Brouwer, D.; Frederiks, C.L.; Falandt, M.; Levato, R.; Kranenburg, O.; Lindemans, C.A.; Coffer, P.J.; et al. Impact of 3D Cell Culture Hydrogels Derived from Basement Membrane Extracts or Nanofibrillar Cellulose on CAR-T Cell Activation. *iScience* **2025**, *28*, 113234, doi:10.1016/j.isci.2025.113234.
28. Valdoz, J.C.; Johnson, B.C.; Jacobs, D.J.; Franks, N.A.; Dodson, E.L.; Sanders, C.; Cribbs, C.G.; Van Ry, P.M. The ECM: To Scaffold, or Not to Scaffold, That Is the Question. *International Journal of Molecular Sciences 2021, Vol. 22, Page 12690* **2021**, *22*, 12690, doi:10.3390/IJMS222312690.
29. Andrews, M.G.; Kriegstein, A.R. Challenges of Organoid Research. *Annu Rev Neurosci* **2022**, *45*, 23, doi:10.1146/ANNUREV-NEURO-111020-090812.
30. Ramesh, P.; Moskwa, N.; Hanchon, Z.; Koplas, A.; Nelson, D.A.; Mills, K.L.; Castracane, J.; Larsen, M.; Sharfstein, S.T.; Xie, Y. Engineering Cryoelectrospun Elastin-Alginate Scaffolds to Serve as Stromal Extracellular Matrices. *Biofabrication* **2022**, *14*, 5, doi:10.1088/1758-5090/AC6B34.
31. Ramesh, P. Biomimetic Scaffolds Targeting Remediation of Fibrosis and Regeneration of the Salivary Gland, SUNY Polytechnic Institute, 2022.
32. Ramesh, P.; Pena, R.; Morrissey, J.M.; Moskwa, N.; Tubbesing, K.; Zhang, X.; Nelson, D.; Castracane, J.; Khmaladze, A.; Sharfstein, S.T.; et al. Cryoelectrospun Elastin-Alginate Scaffolds as Potential Cell Delivery Vehicles for Mesenchymal Stromal Cell Therapy. *Scientific Reports 2025 15:1* **2025**, *15*, 1–18, doi:10.1038/s41598-025-03822-x.
33. Beucler, M.J.; Miller, W.E. Isolation of Salivary Epithelial Cells from Human Salivary Glands for In Vitro Growth as Salispheres or Monolayers. *J Vis Exp* **2019**, *2019*, e59868, doi:10.3791/59868.
34. Jeong, Y.J.; Hong, Y.; Yoon, Y.J.; Sim, N.S.; Hong, S.M.; Lim, J.Y. Chemical Reprogramming Culture for the Expansion of Salivary Gland Epithelial Basal Progenitor Cells. *Stem Cell Res Ther* **2025**, *16*, doi:10.1186/S13287-025-04295-5.
35. Athwal, H.K.; Lombaert, I.M.A. 3D Organoid Formation from the Murine Salivary Gland Cell Line SIMS. *Bio Protoc* **2019**, *9*, e3386, doi:10.21769/BIOPROTOC.3386.
36. Moskwa, N.; Mahmood, A.; Nelson, D.A.; Altrieth, A.L.; Forni, P.E.; Larsen, M. Single-Cell RNA Sequencing Reveals PDFGRα+ Stromal Cell Subpopulations That Promote Proacinar Cell Differentiation in Embryonic Salivary Gland Organoids. *Development* **2022**, *149*, dev200167, doi:10.1242/DEV.200167/274560/AM/SINGLE-CELL-SEQUENCING-REVEALS-PDFGR-STROMAL-CELL.

 doi:10.20944/preprints202511.0438.v1

37. Hosseini, Z.F.; Nelson, D.A.; Moskwa, N.; Sfakis, L.M.; Castracane, J.; Larsen, M. FGF2-Dependent Mesenchyme and Laminin-111 Are Niche Factors in Salivary Gland Organoids. *J Cell Sci* **2018**, *131*, doi:10.1242/JCS.208728.
38. Salimbeigi, G.; Vrana, N.E.; Ghaemmaghami, A.M.; Huri, P.Y.; McGuinness, G.B. Basement Membrane Properties and Their Recapitulation in Organ-on-Chip Applications. *Mater Today Bio* **2022**, *15*, 100301, doi:10.1016/J.MTBIO.2022.100301.
39. Kozyrina, A.N.; Piskova, T.; Di Russo, J. Mechanobiology of Epithelia From the Perspective of Extracellular Matrix Heterogeneity. *Front Bioeng Biotechnol* **2020**, *8*, 1255, doi:10.3389/FBIOE.2020.596599/BIBTEX.
40. Frantz, C.; Stewart, K.M.; Weaver, V.M. The Extracellular Matrix at a Glance. *J Cell Sci* **2010**, *123*, 4195–4200, doi:10.1242/jcs.023820.
41. Bosman, F.T.; Stamenkovic, I. Functional Structure and Composition of the Extracellular Matrix. *J Pathol* **2003**, *200*, 423–428, doi:10.1002/PATH.1437.
42. Lipp, S.N.; Jacobson, K.R.; Hains, D.S.; Schwarderer, A.L.; Calve, S. 3D Mapping Reveals a Complex and Transient Interstitial Matrix During Murine Kidney Development. *Journal of the American Society of Nephrology* **2021**, *32*, 1649–1665, doi:10.1681/ASN.2020081204.
43. Sharfstein, S.; Xie, Y.; Ramesh, P.; Castracane, J.; Larsen, M.; Mosk Compositions, Apparatuses and Methods for Making and Using Bioscaffolds. *United States patent application US 18/108,395* **2024**.
44. Braga, V. Epithelial Cell Shape: Cadherins and Small GTPases. *Exp Cell Res* **2000**, *261*, 83–90, doi:10.1006/EXCR.2000.5050.
45. Laoide, B.M.; Courty, Y.; Gastinne, I.; Thibaut, C.; Kellermann, O.; Rougeon, F. Immortalised Mouse Submandibular Epithelial Cell Lines Retain Polarised Structural and Functional Properties. *J Cell Sci* **1996**.
46. Liu, X.; Sun, Q.; Wang, Q.; Hu, C.; Chen, X.; Li, H.; Czajkowsky, D.M.; Shao, Z. Epithelial Cells in 2D and 3D Cultures Exhibit Large Differences in Higher-Order Genomic Interactions. *Genomics Proteomics Bioinformatics* **2021**, *20*, 101, doi:10.1016/J.GPB.2020.06.017.
47. Donjacour, A.A.; Cunha, G.R. Stromal Regulation of Epithelial Function. *Cancer Treat Res* **1991**, *53*, 335–364, doi:10.1007/978-1-4615-3940-7_16.
48. Güney, T.G.; Herranz, A.M.; Mumby, S.; Dunlop, I.E.; Adcock, I.M. Epithelial–Stromal Cell Interactions and Extracellular Matrix Mechanics Drive the Formation of Airway-Mimetic Tubular Morphology in Lung Organoids. *iScience* **2021**, *24*, 103061, doi:10.1016/j.isci.2021.103061.
49. Jainchill, J.L.; Aaronson, S.A.; Todaro, G.J. Murine Sarcoma and Leukemia Viruses: Assay Using Clonal Lines of Contact-Inhibited Mouse Cells. *J Virol* **1969**, doi:10.1128/jvi.4.5.549-553.1969.
50. de Paula, F.; Teshima, T.H.N.; Hsieh, R.; Souza, M.M.; Nico, M.M.S.; Lourenco, S.V. Overview of Human Salivary Glands: Highlights of Morphology and Developing Processes. *Anat Rec* **2017**, *300*, 1180–1188, doi:10.1002/AR.23569.
51. Campbell, H.K.; Maiers, J.L.; DeMali, K.A. Interplay Between Tight Junctions & Adherens Junctions. *Exp Cell Res* **2017**, *358*, 39, doi:10.1016/J.YEXCR.2017.03.061.
52. Danielsson, F.; Peterson, M.; Caldeira Araújo, H.; Lautenschläger, F.; Gad, A. Vimentin Diversity in Health and Disease. *Cells* **2018**, *7*, 147, doi:10.3390/cells7100147.
53. Trappmann, B.; Gautrot, J.E.; Connelly, J.T.; Strange, D.G.T.; Li, Y.; Oyen, M.L.; Cohen Stuart, M.A.; Boehm, H.; Li, B.; Vogel, V.; et al. Extracellular-Matrix Tethering Regulates Stem-Cell Fate. *Nat Mater* **2012**, *11*, 642–649, doi:10.1038/nmat3339.
54. Sonbol, H. Extracellular Matrix Remodeling in Human Disease. *J Microsc Ultrastruct* **2018**, doi:10.4103/jmau.jmau_4_18.
55. Bonnans, C.; Chou, J.; Werb, Z. Remodelling the Extracellular Matrix in Development and Disease. *Nat Rev Mol Cell Biol* **2014**, *15*, 786–801, doi:10.1038/nrm3904.
56. Soscia, D.A.; Sequeira, S.J.; Schramm, R.A.; Jayarathanam, K.; Cantara, S.I.; Larsen, M.; Castracane, J. Salivary Gland Cell Differentiation and Organization on Micropatterned PLGA Nanofiber Craters. *Biomaterials* **2013**, doi:10.1016/j.biomaterials.2013.05.061.
57. Foraida, Z.I.; Kamaldinov, T.; Nelson, D.A.; Larsen, M.; Castracane, J. Elastin-PLGA Hybrid Electrospun Nanofiber Scaffolds for Salivary Epithelial Cell Self-Organization and Polarization. *Acta Biomater* **2017**, *62*, 116–127, doi:10.1016/j.actbio.2017.08.009.

58. Kwon, S.; Ryu, J.H.; Kim, J.; Shin, H.H.; Chung, G.; Taghizadeh, A.; Lee, J.-H.; Kim, J.; Ku, B.-C.; Park, K.; et al. Biomimetic Catechol-Incorporated Polyacrylonitrile Nanofiber Scaffolds for Tissue Engineering of Functional Salivary Glands. *Biomater Res* **2025**, *29*, doi:10.34133/BMR.0226.
59. Song, Y.; Uchida, H.; Sharipol, A.; Piraino, L.; Mereness, J.A.; Ingalls, M.H.; Rebhahn, J.; Newlands, S.D.; DeLouise, L.A.; Ovitt, C.E.; et al. Development of a Functional Salivary Gland Tissue Chip with Potential for High-Content Drug Screening. *Commun Biol* **2021**, *4*, doi:10.1038/s42003-021-01876-x.
60. Pradhan-Bhatt, S.; Harrington, D.A.; Duncan, R.L.; Jia, X.; Witt, R.L.; Farach-Carson, M.C. Implantable Three-Dimensional Salivary Spheroid Assemblies Demonstrate Fluid and Protein Secretory Responses to Neurotransmitters. *https://home.liebertpub.com/tea* **2013**, *19*, 1610–1620, doi:10.1089/TEN.TEA.2012.0301.
61. Jean-Gilles, R.; Soscia, D.; Sequeira, S.; Melfi, M.; Gadre, A.; Castracane, J.; Larsen, M. Novel Modeling Approach to Generate a Polymeric Nanofiber Scaffold for Salivary Gland Cells. *J Nanotechnol Eng Med* **2010**, doi:10.1115/1.4001744.
62. Wells, K.L.; Gaete, M.; Matalova, E.; Deutsch, D.; Rice, D.; Tucker, A.S. Dynamic Relationship of the Epithelium and Mesenchyme during Salivary Gland Initiation: The Role of Fgf10. *Biol Open* **2013**, *2*, 981, doi:10.1242/BIO.20135306.
63. Sathi, G.A.; Farahat, M.; Hara, E.S.; Taketa, H.; Nagatsuka, H.; Kuboki, T.; Matsumoto, T. MCSF Orchestrates Branching Morphogenesis in Developing Submandibular Gland Tissue. *J Cell Sci* **2017**, *130*, 1559–1569, doi:10.1242/JCS.196907/265280/AM/MCSF-ORCHESTRATES-BRANCHING-MORPHOGENESIS-IN.
64. Marinkovic, M.; Tran, O.N.; Wang, H.; Abdul-Azees, P.; Dean, D.D.; Chen, X.D.; Yeh, C.K. Extracellular Matrix Turnover in Salivary Gland Disorders and Regenerative Therapies: Obstacles and Opportunities. *J Oral Biol Craniofac Res* **2023**, *13*, 693–703, doi:10.1016/J.JOBCR.2023.08.009.
65. Tavarez, J.R.; Kenney, J.; Gabunia, S.; Nelson, D.A.; Larsen, M. Temporal Evolution of Fibroblast Responses Following Salivary Gland Ductal Ligation Injury. *Frontiers in Dental Medicine* **2025**, *6*, 1581376, doi:10.3389/FDMED.2025.1581376/BIBTEX.
66. Bissell, D.M. Chronic Liver Injury, TGF-β, and Cancer. *Experimental & Molecular Medicine 2001 33:4* **2001**, *33*, 179–190, doi:10.1038/emm.2001.31.
67. Hupfer, A.; Brichkina, A.; Koeniger, A.; Keber, C.; Denkert, C.; Pfefferle, P.; Helmprobst, F.; Pagenstecher, A.; Visekruna, A.; Lauth, M. Matrix Stiffness Drives Stromal Autophagy and Promotes Formation of a Protumorigenic Niche. *Proc Natl Acad Sci U S A* **2021**, *118*, e2105367118, doi:10.1073/PNAS.2105367118/SUPPL_FILE/PNAS.2105367118.SAPP.PDF.
68. O'Connor, J.W.; Gomez, E.W. Biomechanics of TGFβ-Induced Epithelial-Mesenchymal Transition: Implications for Fibrosis and Cancer. *Clinical and Translational Medicine 2014 3:1* **2014**, *3*, 1–13, doi:10.1186/2001-1326-3-23.
69. Liu, P.; Zhang, D.; Huang, G.; Xue, M.; Fang, Y.; Lu, L.; Zhang, J.; Xie, M.; Ye, Z. Laminin A1 as a Target for the Treatment of Epidural Fibrosis by Regulating Fibrotic Mechanisms. *Int J Mol Med* **2023**, *51*, 1–11, doi:10.3892/IJMM.2022.5205/HTML.
70. Peters, S.B.; Naim, N.; Nelson, D.A.; Mosier, A.P.; Cady, N.C.; Larsen, M. Biocompatible Tissue Scaffold Compliance Promotes Salivary Gland Morphogenesis and Differentiation. *Tissue Eng Part A* **2014**, *20*, 1632, doi:10.1089/TEN.TEA.2013.0515.